Diamond & Related Materials 106 (2020) 107842

Contents lists available at ScienceDirect

Diamond & Related Materials

journal homepage: www.elsevier.com/locate/diamond

Characterization of interfacial bonding strength at Al(Si)/diamond interfaces by neutron diffraction: Effect of diamond surface termination and processing conditions

Christian Edtmaier[a,*], Jakob Segl[a], Robert Koos[b], Michael Schöbel[b,c], Christoph Feldbaumer[a]

[a] TU Wien, Institute of Chemical Technologies and Analytics, Getreidemarkt 9, 1060 Vienna, Austria
[b] Technische Universität München, Heinz-Maier-Leibnitz Zentrum FRM II, Lichtenbergstr. 1, 85747 Garching, Germany
[c] X-ray Center (XRC), TU Wien, Getreidemarkt 9, 1060 Vienna, Austria

ABSTRACT

Interfacial bonding plays a vital role and is of eminent importance for thermo-physical and mechanical properties in particulate and fibrous composites. Moreover, the formation of interfacial carbides in the reactive system Al/diamond dominates the thermal and mechanical response. The amount of interfacial carbides can be controlled by the nominal composition of the matrix and process parameters like contact times between the liquid aluminium and the diamond particles during and the surface termination of the diamonds before the liquid metal infiltration processing. Neutron diffraction experiments were performed to study the influence of those parameters on interfacial bonding strength and show a direct correlation between thermo-physical properties, concentration of interfacial aluminium-carbide Al_4C_3 and micro strain concentrations during neutron diffraction experiment. Furthermore, the oxygenation of the diamond particle surface has a major contribution to the interfacial bonding and thermal conductivity of the composites, respectively. This effect, however, almost diminishes when Al3Si is used as a matrix.

1. Introduction

Considering a general high mismatch in coefficients of thermal expansion CTE between typical inclusions like silicon-carbide SiC, alumina Al_2O_3, boron-carbide B_4C and diamond CD and a metallic matrix like aluminium and Al alloys, high micro stresses and strains in the matrix alloy and at the interfaces may initiate matrix deformation and thermal fatigue damage of the metal matrix composites (MMCs) [1–3]. This can be also attributed to the change in temperatures while cooling from processing or from thermal cycling during operation. As shown by Schöbel et al. [2] micro-stresses upon cooling may lead to delamination at the interfaces, but also to the creation of pores within the matrix. Furthermore, the micro-stress evolution is also responsible for the reduction in thermal conductivity of the composites. Thus, interfacial bonding strength is a key issue to ensure sufficient long-term stability during operation.

Processing conditions in the preparation of metal/diamond composites can play a crucial role, as previously shown by Monje [4,5] and Edtmaier [6]. The increasing formation of excess interfacial carbides with increasing contact time between the liquid metal and the diamond particles in the gas pressure infiltration process tend to negatively influence composite thermal conductivity. Note, that a minimum amount of aluminium-carbide Al_4C_3 at the diamond–metal interface appears to be a basic necessity to create interfacial bonding and thus thermal transport across the interface, as composite thermal conductivity will be low when interfacial carbides are absent [7]. Furthermore, it was also previously shown [8–10], that surface termination plays another important role in bonding strength and thermal transport between the constituents. It appeared that oxygenated surfaces could result in favourable thermal boundary conductances between diamonds and metallic matrices compared to systems with hydrogenated diamond surfaces. The addition of carbide forming elements to the matrix and coating of the diamond particles respectively are other strategies to overcome thermal transport problems across the interface caused by weak interfacial bonding and as observed in copper/diamond (Cu/CD) [11,12], silver/diamond (Ag/CD) [9,13] and aluminium/diamond (Al/CD) [7,14], respectively. Chen and co-workers [15] claimed, that high thermal conductivity is concomitantly associated with high bending strength in Al/CD composites. This relationship implies that interfacial bonding strength plays an important role in the thermal transport characteristics in composites.

Bonding strength between inclusion and matrix in a composite can be hardly measured directly and thermo-physical behaviour of composites is just an indirect measure for the quality of composites and interfaces. In this work we aimed to shed some light on interfacial bonding strength by neutron diffraction experiments to compare the results with thermo-physical properties of the composites and theoretical predictions of the interface conductance. Neutron diffraction

* Corresponding author.
E-mail address: christian.edtmaier@tuwien.ac.at (C. Edtmaier).

https://doi.org/10.1016/j.diamond.2020.107842
Received 27 February 2020; Received in revised form 30 March 2020; Accepted 3 April 2020
Available online 06 April 2020

reveals micro-strains between diamond particles and Al and Al3Si matrices, respectively, as a function of nominal matrix composition, processing and diamond surface conditions related to thermal conductivity and interfacial carbide Al_4C_3 formation. The experimental work was performed on the Stress-Spec strain scanner [16] at the high flux source FRM2 in Garching, Germany.

2. Experimental procedure

Diamond composites were produced by liquid metal infiltration of Al and Al3Si base material into a tapped and vibrated powder bed of synthetic diamond grits of mesh size 230/270 (Ø ~ 53–63 μm). The matrix alloy was primarily inductively melted and cast of 3 N8 Al and 4 N Si base elements. The Si concentration in the Al was adjusted to three wt.-pct. The synthetic diamonds were purchased from *ServSix GmbH, Karlstein, Germany* and were of the SDB 1125 type from E6. Such type of diamonds is a commercially available quality that performs with highest crystallinity, particle strength and lowest impurities, thus representing diamond powders of highest thermal conductivity.

Diamond particles are used in the as received (denoted subsequently as “pristine”), in the hydrogen terminated (CD:H) and oxygen (CD:O) terminated conditions. To create CD:H termination on the diamond surfaces, the powders were exposed to H_2 gas atmosphere for 60 min in a furnace at 1123 K. CD:O termination was realized by immersing diamonds in hot sulphuric acid for a period of 5 min, subsequently rinsed with de-ionized water and 2-propanol and finally dried at 383 K.

The thermal conductivity and tensile test specimens for the neutron diffraction experiments were infiltrated net-shape. Geometrical details of the tensile specimens are given in Fig. 1a, the overall test setup in the Stress-Spec instrument can be seen in Fig. 1b. The test specimen for thermal conductivity investigations are rods of 8 mm diameter and an overall length of about 33 mm. Solid pieces of metal and metal alloy, respectively, were placed on top of the graphite preform filled up with diamond particles. Prior to melting, a vacuum was applied in order to facilitate infiltration. After the infiltration temperature of roughly 1173 K had been reached, Argon gas pressure of 3 MPa was applied to force the liquid metal into the diamond powder bed. The heating was switched off after 1 min and 10 min (which is called the “contact time” t_c between the liquid and the diamonds) and the infiltrated bodies were furnace cooled under pressurized condition within < 20 min to room temperature. After cooling down, composite pieces were dismantled from the die.

The diamond volume fraction was determined by densitometry to be 59 ± 1 vol.-pct for all MMCs. This is in good agreement with the relative densities of up to 99.5 pct., indicating that the composite samples were fully infiltrated and contained little, if any, porosity.

Thermal conductivity measurements were performed in a steady-state heat flow equipment close to ambient temperature, quantitative analysis of the interfacial amount of Al_4C_3 was performed by gas chromatography–mass spectrometry GC–MS. For a detailed description of the experimental methods we refer to a previous paper [6].

The load carrying capacity of diamonds in Al composites and in particular the interface between those constituents was investigated by neutron diffraction as a function of processing parameters, i.e. the contact time between the liquid metal and the diamonds during infiltration, moreover the nominal composition of the matrix and the surface termination of the used diamond particles. Neutron diffraction experiments were performed to determine micro-strains between matrix and diamond particles in-situ during tensile tests using a customized tensile test rig [17] and were performed in the Stress-Spec instrument [16] of the high flux neutron source FRM2, Garching, Germany. The Stress-Spec set-up (Fig. 2a) allows strain scans on the Al (311) and CD (220) lattice planes in the matrix and the diamonds with an acquisition time of 120 s in an approx. 125 mm^3 (5 × 5 × 5 mm^3) gauge volume. A representative volume is necessary to sample a statistically relevant number of grains contributing to the diffraction peak of the coarse grained matrix.

During all experiments the 2D ^{3}He detector [18] (256 × 256 pixels) was set to 86° (center position), including Al (311) at 2θ ~ 86.5° and CD (220) at 2θ ~ 83.5°. Summation along the projected Debye-Scherrer rings according to [19] gave the peaks relative to the reference. The elastic strains were determined in-situ during tensile tests. The gauge volume containing several diamond particles embedded in the matrix gave an averaged matrix and diamond strain value. The three principal strain orientations ε_i exhibit spherical symmetry with particle sizes smaller than the gauge volume, as shown in [1].

The external tensile force was controlled by a calibrated load cell. Starting from an initially preloaded condition of 200 N, the load was incrementally increased by each 400 N and kept constant at each step for an acquisition time of 120 s to allow scanning the Al and AlSi matrices (311) and diamond (220) peak intensities, before unloading for another 120 s (Fig. 2b). In the unloaded condition, the initial micro-stress state from casting (cooling after infiltration) was neglected.

3. Results and discussion

Before considering neutron diffraction experimental investigations and results, the impact of processing conditions during the infiltration process, i.e. contact time between the liquid metal and the diamonds, furthermore, nominal matrix composition and diamond surface termination respectively on thermal conductivity behaviour and interfacial carbide formation has to be discussed. Table 1 lists thermo-physical properties of all investigated specimens prepared for the neutron diffraction experiments.

Comparing the thermal conductivity of the pure Al/CD composites at 1 min contact time it is clearly visible, that surface termination plays

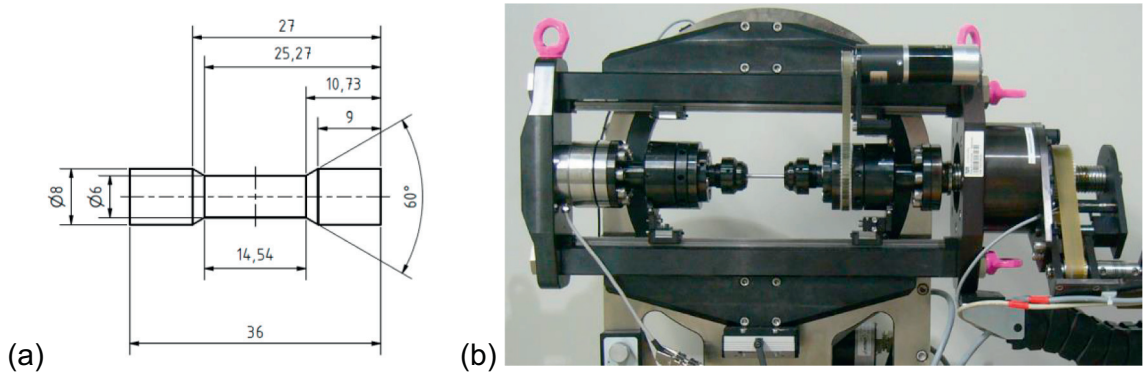

Fig. 1. Al/CD/59p and Al3Si/CD/59p tensile test specimen geometry for neutron diffraction experiments fabricated by gas pressure infiltration of diamond particles with pure Al and Al3Si alloy (a) and tensile test setup [17] in the Stress-Spec instrument at FRM II (b).

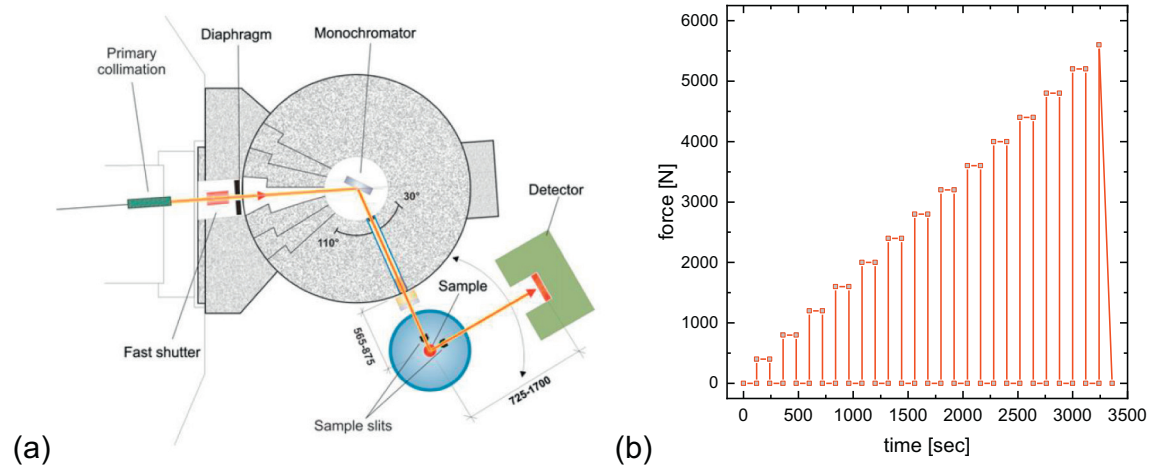

Fig. 2. Sketch of the Stress-Spec instrumental set-up at FRM2 [2]. A Si double focusing single crystal monochromator [20] filters a wavelength of $\lambda = 1.67$ Å from thermal neutrons using the Si(400) lattice of a focussing bent single crystal Si monochromator at a flux of 2–3 $\times 10^7$ n cm^{-2} s^{-1} on the sample with acquisition times of 120 s (a). The tensile tests and neutron diffraction analysis were performed during loading and unloading intervals. Each load was kept constant for 120 s before unloading. Diffraction scans during loading and after unloading conditions correspond to in-situ and ex-situ measurements, respectively (b).

a role, as thermal conductivity increases when diamond surfaces are oxygenated compared to both the as-received (untreated) diamond particles and H-terminated diamonds. The same behaviour is observable for a contact time of 10 min, as MMCs with oxygenated diamonds exhibit the highest conductivity compared to the H-terminated and untreated ones. When comparing the Al/CD and Al3Si/CD composites it is noticeable that the thermal conductivity is generally lower for the Al3Si matrix composites. As the difference in matrix thermal conductivity κ_m between pure aluminium and Al3Si amounts to 18 W m^{-1} K^{-1} (κ_m of pure aluminium was found to be 235 ± 2 W m^{-1} K^{-1}, compared to 217 ± 1 W m^{-1} K^{-1} for Al3Si), this difference cannot be solely responsible for the observed decrease in composite conductivity between Al/CD and Al3Si/CD composites. The conductivity within the series of Al3Si of 1 min and 10 min, respectively, follows a similar trend as for the pure Al/CD series, i.e. higher conductivity for oxygen terminated diamonds compared to H-terminated and as-received ones, although this effect is not very pronounced for 1 min contact time.

Furthermore, similar behaviour is observed between the two series of 1 min and 10 min contact time for Al3Si/CD: the composite thermal conductivity is generally lower for the 10 min contact time, independently of the surface termination.

In general, the CD:H terminated diamonds show the lowest κ_c of all investigated MMCs, with the most distinct decline of approx. 20 pct. for a contact time of 10 min and three wt.-pct. of Si in Al compared to the κ_c of the materials using the as-received and those using CD:O terminated diamonds.

For the calculation of h according to the DEM scheme we refer to a previous paper [6]. The data used for the predictions are: radius of inclusion $a = 30$ µm, volume fraction of diamond particles $V_i = 0.59$ and thermal conductivity of diamond $\kappa_{CD} = 1587$ W m^{-1} K^{-1}. This thermal conductivity for CD was derived by measurement of the nitrogen concentration measured by combustion method and which amounted to be 341 ± 10 ppm nitrogen. From this, the thermal conductivity was calculated by the expression proposed by Yamamoto [21].

In a recent paper [6], it was certified that the thermo-physical behaviour of Al/CD composites is a function of the interfacial Al_4C_3 carbides formation, as the contact times and thermal conductivity results correlate with the aluminium-carbide concentrations. In this present study a similar tendency can be observed, as the quantitative analysis of the interfacial carbides in dependence of the processing conditions and matrix composition for Al/CD and Al3Si/CD with 230/270 mesh sized diamonds showed the same trend, Table 1.

Furthermore, it is known from previous studies that the addition of Si to Al may effectively suppress the formation of Al_4C_3 by the preferential formation of SiC (Eq. (3)). However, it is also possible, that by subsequent reaction, some ("free") Si and Al_4SiC_4 phases, respectively, may be generated according Eq. (4) and (5):

$$4Al + 4C + Si \rightleftharpoons Al_4C_3 + SiC \quad (1)$$

$$4Al + 3SiC \rightleftharpoons 3Si + Al_4C_3 \quad (2)$$

$$Al_4C_3 + SiC \rightleftharpoons Al_4SiC_4 \quad (3)$$

Table 1 clearly show both effects, i.e. a decrease in Al_4C_3 while increasing the contact time and a suppression of excess Al_4C_3 formation by the addition of Si. Moreover, the O-termination of diamond surfaces is responsible for a very effective reduction of interfacial carbide formation. This is more pronounced for Al/CD, than Al3Si/CD, where the effect of oxygenation almost diminishes.

Table 1
Composite thermal conductivity κ_c, calculated interface thermal conductance (ITC) h according differential effective medium (DEM) scheme and interfacial Al_4C_3 concentration of the investigated Al/CD/59p and Al3Si/CD/59p composites at 1 min and 10 min contact time t_c using as received ("pristine"), CD:O oxygenated and CD:H hydrogenated diamond particles of mesh size 230/270.

Matrix	Diamond surface termination	Contact time t_c (min)	Composite thermal conductivity κ_c (W m^{-1} K^{-1})	ITC h (DEM) (W m^{-2} K^{-1})	Al_4C_3 (wt.-pct.)
Al	CD-„pristine“	1	373 ± 1	2.43E+7	4.58 ± 0.046
Al	CD:O	1	455 ± 6	4.02E+7	3.75 ± 0.031
Al	CD:H	1	376 ± 8	2.48E+7	5.07 ± 0.074
Al	CD-„pristine“	10	283 ± 7	1.34E+7	7.92 ± 0.087
Al3Si	CD-„pristine“	1	295 ± 6	1.55E+7	3.91 ± 0.046
Al3Si	CD:O	1	305 ± 1	1.66E+7	3.29 ± 0.01
Al3Si	CD:H	1	290 ± 3	1.49E+7	3.32 ± 0.018

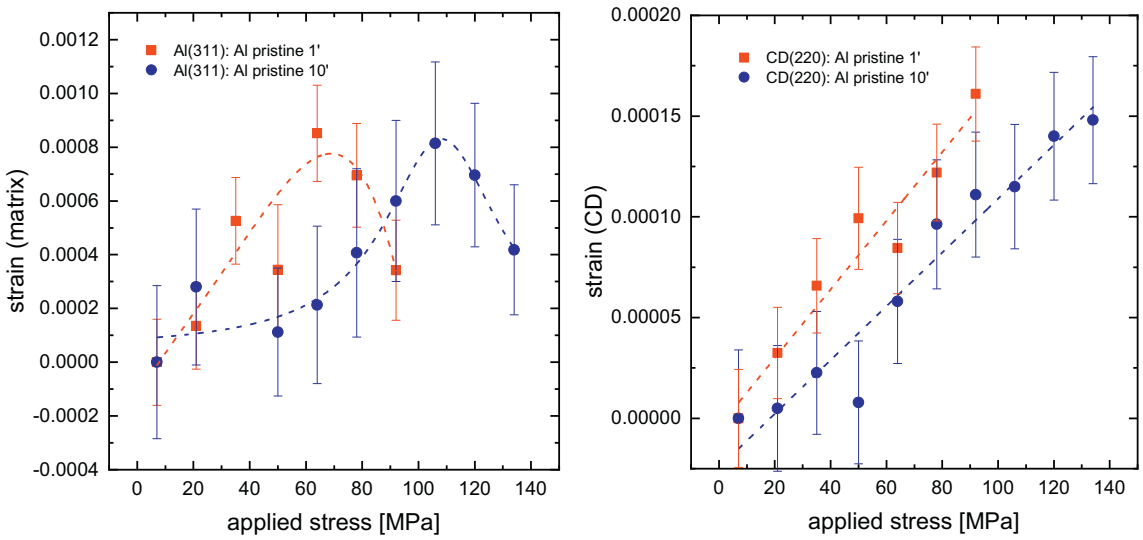

Fig. 3. Tensile tests on Al/CD/59p at 1 min and 10 min a contact time between liquid Al and diamond particles during infiltration, respectively; In-situ (axial) micro strains in (a) Al matrix (311) and (b) in diamond (220). The dotted lines represent the polynomial and linear fits of data associated to the respective different contact times.

The impact of interfacial carbides and contact time on the mechanical response in the neutron diffraction experiment can be identified in Fig. 3. The parallel strain evolution between Al matrix and diamond particles indicates elastic deformation of both the metallic matrix and the diamond inclusions in the in-situ measurement in axial direction.

As indicated above, the increase in contact time induces increased carbide formation (Table 1). Interestingly, this furthermore induces a higher load transfer from the ductile metallic matrix into the diamond particles, as this obviously improves bonding strength between matrix and diamonds. This is visible by an increase in fracture load from 92 MPa to 134 MPa (at approx. the same fracture strain) between composites of 1 min and 10 min contact time (Fig. 3). From this, we deduce improved interfacial bonding strength between diamond and matrix upon formation of interfacial carbides. Note, that this is associated with a decrease in composite thermal conductivity, as the higher amount of interfacial carbides at 10 min contact time leads to higher interfacial resistance, thus reduced interface thermal transport.

The parallel strain evolution between Al matrix and diamond particles (Fig. 3 a & b) indicates elastic deformation of both the metallic matrix and the diamond inclusions (in-situ measurement in axial direction). The ex-situ measurements represent the unloaded condition at the different stress levels and indicate residual micro deformation in the Al matrix up to a low stress level for both the 1 min and 10 min contact time, Fig. 4a. Whereas Fig. 4b shows residual deformation in the diamond particles to be neglected.

Increasing the contact time between the liquid and the diamond particles during infiltration operation induces increased carbide formation in Table 1. This furthermore induces a higher load transfer from the ductile metallic matrix into the diamond particles, as this obviously improves bonding strength between matrix and diamonds. An increase in fracture load can be observed from 92 MPa to 134 MPa (at approx. the same fracture strain) between Al/CD composites of 1 min and 10 min contact time (Fig. 3), thus improved interfacial bonding strength between diamond and matrix upon formation of interfacial carbides can be assumed. Interestingly this increase in bonding strength is associated with a decrease in composite thermal conductivity κ_c, provoked by a higher interfacial resistance and reduced interface thermal transport due to an increasing concentration of interfacial carbides at 10 min contact time.

As a matter of fact, we see a peak in matrix strain with increasing applied stresses for both contact times of 1 min (at approx. 60–70 MPa) and 10 min (at approx. 100–110 MPa) respectively (Fig. 3a). Linear behaviour appears in (220) diamond strains and with increasing applied stresses. We conclude elasto-plastic deformation of the matrix up to those maxima, but at the strain peak, either the matrix softens or the interface between the diamonds and the metallic matrix weakens and partly delaminates, resulting in the observed decrease in matrix strain. Concomitantly the diamonds are linearly deformed until rupture without any peak and decrease in strain. We further conclude that no total delamination between the constituents with some remaining interaction must be still present with deformation hardening of the matrix in the end, as diamonds would not linearly deform until rupture, if there is full delamination. The elastic deformation of diamonds (elongation of the diamonds) relies on a certain residual adhesion between diamond and matrix, since otherwise no forces could be transmitted with further increasing load.

When comparing ex-situ and in-situ data in Fig. 3 a/b and Fig. 4 a/b, we can learn, that the matrix strain in the unloaded condition is almost zero at approx. 50–70 MPa. We conclude mainly elastic matrix deformation under loading, completely relaxing during unloading without any residual stress contribution if external stress stays below matrix yield strength < 70 MPa. Nevertheless partial interfacial plastification of the matrix alloy may lead to low strain amounts for 1 and 10 min contact time, whereas at stresses above approx. 70 MPa no strains can be observed for 10 min contact time and very low ones for 1 min. Interestingly, this total release of matrix strain in the ex-situ data of 10 min contact time coincides with the increase in matrix strain of the in-situ results of the same composite material.

As shown by Schöbel et al. [22] a heat treatment of the particle preform in Al/CD composites may have the same effect of improving bonding strength as shown above by the increasing contact time. The authors argued, that the ductile aluminium matrix starts to flow above the elastic region and deforms plastically until fracture. This indicates an overall stiff but partial ductile deformation behaviour of the Al/CD composites, whereas in the heat treated condition the MMCs have a significantly higher fracture strain. They conclude, that the heat treatment induces interfacial carbide formation improves bonding strength at the particle-matrix interface, although no quantitative analysis for interfacial carbides was available.

When considering a different matrix composition by introducing three wt.-pct. of Si in Al the elasto-plastic matrix behaviour at 1 min contact time significantly changes, Fig. 5 indicates, the maximum fracture load increasing from 92 MPa for Al/CD to 177 MPa for the

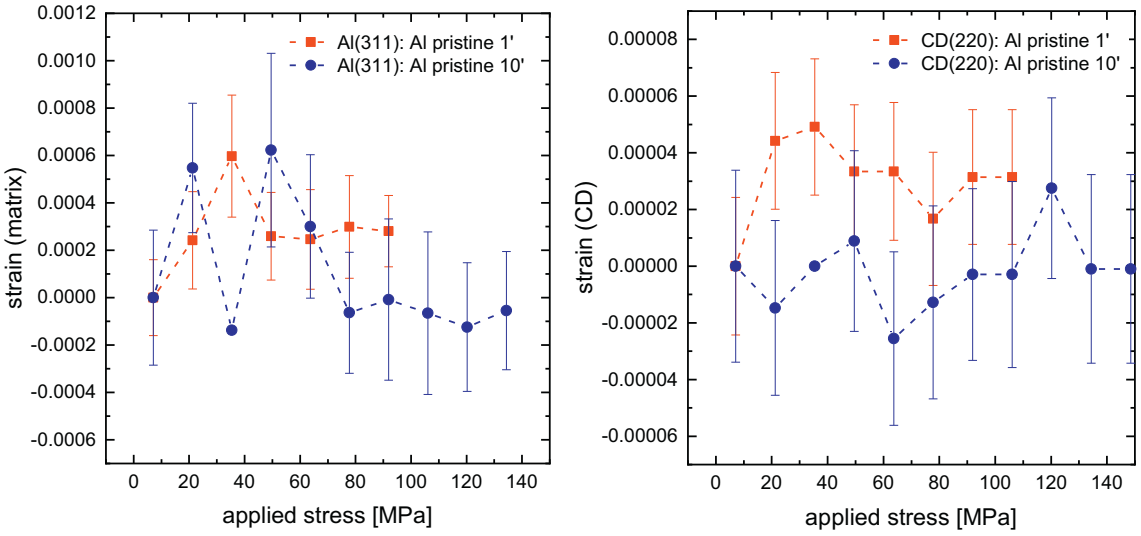

Fig. 4. Tensile test on Al/CD/59p at 1 min and 10 min contact time between liquid Al and diamond particles during infiltration, respectively; Ex-situ (axial) micro strains in (a) Al matrix (311) and (b) in diamond (220).

Al3Si/CD. This is also a one-third increase in fracture load for Al3Si/CD at 1 min contact time compared to 10 min for Al/CD. Obviously, the addition of Si has a high impact, as the bonding strength between the stiff diamond particles and the elasto-plastic deforming matrix increases with increasing load. This is provoked by suppression of interfacial carbides and due to the formation of interfacial SiC and Al_4SiC_4, respectively (Eq. (3)). Furthermore, a peak in matrix strain is visible at approx. 60–70 MPa for the pure Al/CD composite and approx. 140–150 MPa for the Al3Si/CD one.

When we introduce different surface terminations on diamond surfaces the deformation behaviour again changes, as the fracture load increases for oxygenated diamonds in 1 min contact time Al/CD composites compared to the pristine and the CD:H terminated ones (Fig. 6). This is consistent with thermo-physical properties in Table 1, where the Al:O 1 min composite has a significant higher thermal conductivity compared to the pristine and CD:H terminated ones. The matrix strain evolution with increasing load of the oxygenated specimen is almost negligibly small, due to weak load transfer between matrix and diamonds.

When transferring different diamond surface conditions to Al3Si/CD composites (Fig. 7) we can observe a very similar behaviour for all three different conditions. This is consistent with the thermo-physical data in Table 1, as the thermal conductivities and the concentration of interfacial carbides for Al3Si/CD are in a very close range for composites with pristine, hydrogenated and oxygenated diamonds. This may be due to the pronounced effect of Si that is responsible for the suppression of the Al_4C_3 formation and that is even more distinct, than the diamond surface condition.

The amount of hydrolysed interfacial carbides was used for quantitative analysis. If we compare the fracture surfaces of the broken tensile test specimens of the composite prepared by 1 min and 10 min contact time in Fig. 8 we can easily identify different amounts of “fluffy” reaction products of the original interfacial carbides. This is much more pronounced for the 10 min composite compared to the 1 min specimen. In the Al3Si/CD this flaky products are less, compared to the Al/CD fracture surface.

The fracture surfaces of the broken tensile test specimens of the composite prepared by 1 min and 10 min contact time are compared in

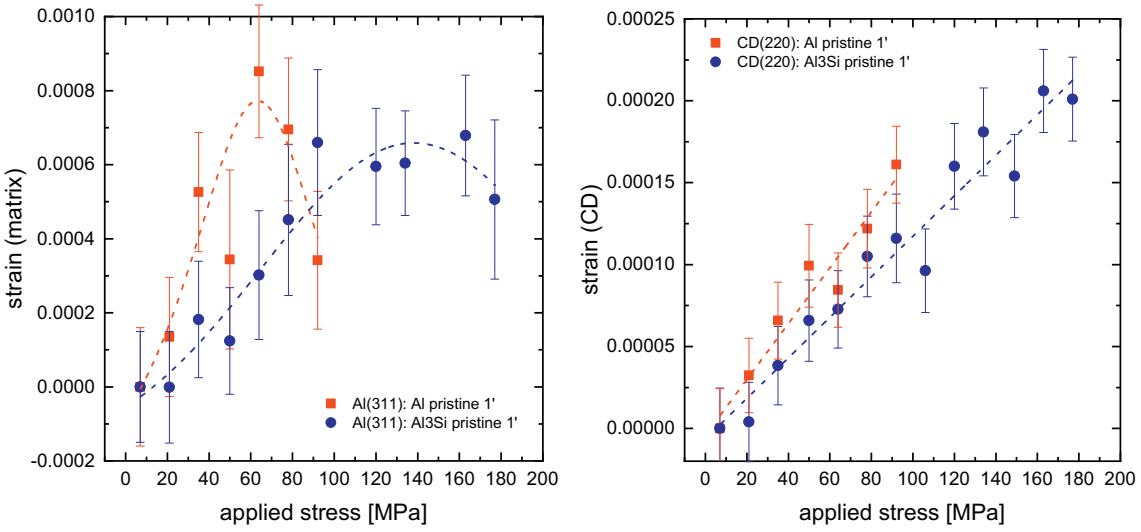

Fig. 5. Tensile tests on Al/CD/59p and Al3Si/CD/59p at a contact time between liquid Al and diamond particles during infiltration of 1 min, in-situ (axial) (a) micro strain in Al and Al3Si matrices (311) and (b) in diamond (220). The dotted lines represent the polynomial and linear fits of data associated to the respective different matrix compositions.

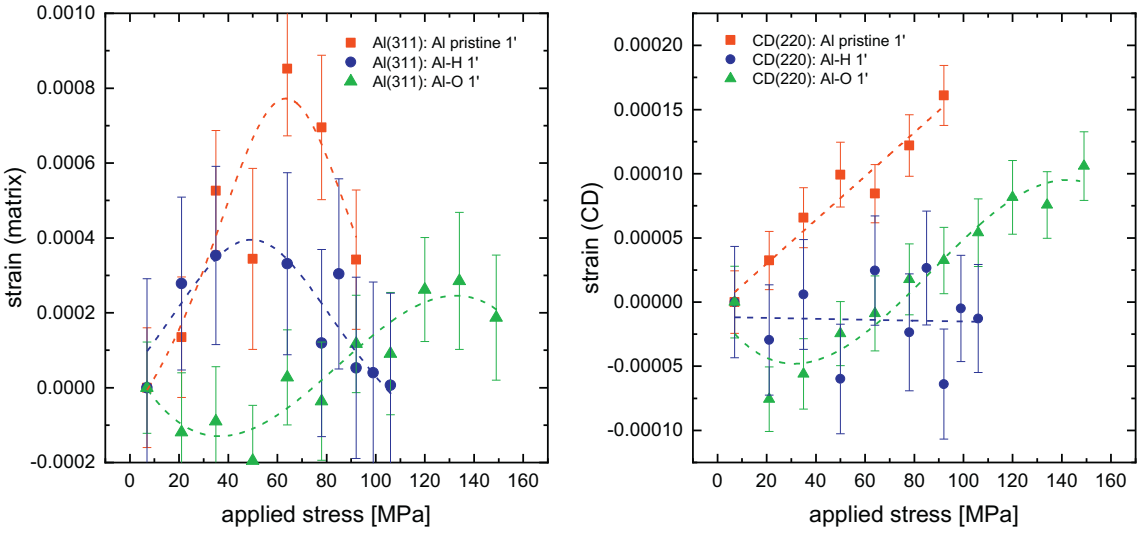

Fig. 6. Tensile tests on Al/CD/59p at a contact time between liquid Al and diamond particles during infiltration of 1 min, the graph compares the as-delivered ("pristine"), CD:H terminated and CD:O terminated diamond particle surfaces in the respective MMCs, in-situ (axial) (a) micro strain in Al matrix (311) and (b) in diamond (220). The dotted lines represent the polynomial and linear fits of data associated to the respective different surface terminations.

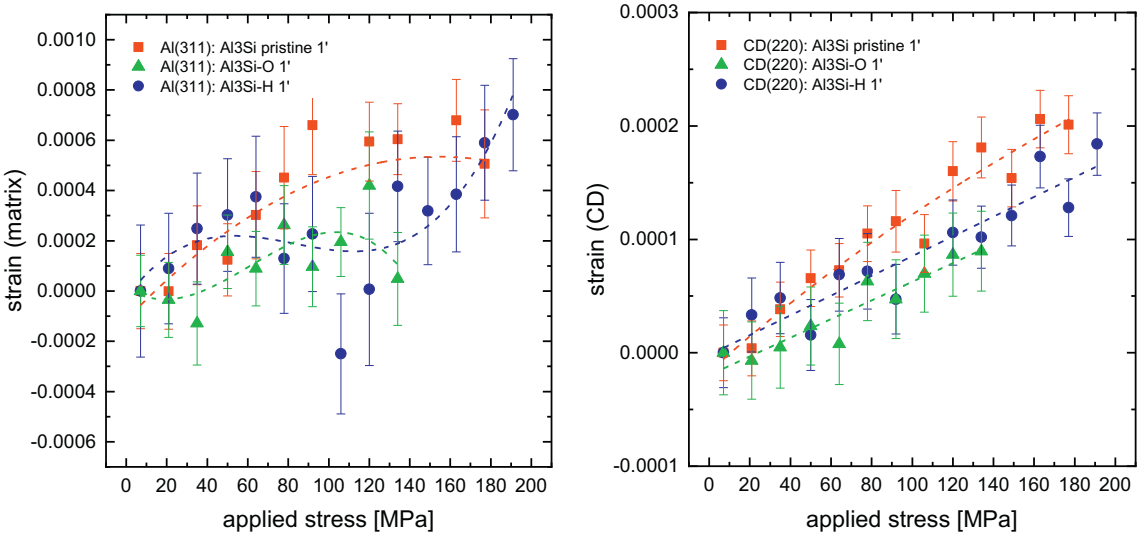

Fig. 7. Tensile tests on Al/CD/59p at a contact time between liquid Al3Si and diamond particles during infiltration of 1 min, the graph compares the as-delivered ("pristine"), CD:H terminated and CD:O terminated diamond particle surfaces in the respective MMCs, in-situ (axial) (a) micro strain in Al3Si matrix (311) and (b) in diamond (220). The dotted lines represent the polynomial and linear fits of data associated to the respective different surface terminations.

Fig. 8, where we can identify different amounts of "fluffy" reaction products of the original interfacial carbides by time delayed sample storage after neutron irradiation. The tensile test samples had to be stored for several days in containment to ensure activated material decay and avoid environmental contamination. Therefore the fracture surfaces appear slightly covered with hydrolysed (mainly sensitive Al4C3 phases) and oxidised interfacial carbides in these "fluffy" phases. Nevertheless, the plastically deformed Al matrix shows a network of dimples, typical for the ductile behaviour of pure metals and which is comparable to the described fracture surfaces in [22]. All interfaces between matrix and diamond particles show sufficient interfacial bonding, except the Al/CD-pristine 1 min composite, which exhibits partly unaffected diamond planes. In the Al3Si/CD series in Fig. 8 the character of fracture is different to the Al/CD one as no dimples and a Si skeleton in the Al phase are visible. Moreover, the addition of Si to Al suppresses the formation of Al_4C_3, thus, less hydrolysed reaction products are visible in the fractured surfaces.

Interfacial bonding strength has been experimentally investigated, although direct measurements of interfacial mechanical strength appear to be an experimental challenge. Time-domain thermoreflectance (TDTR) setup is a common experimental arrangement to draw conclusions from interfacial thermal conductances to bonding strength between different sputtered layers on substrates, which in consequence may also allow to draw conclusions in some respect to the interfacial adhesive behaviour of constituents in "real" composites. Anyhow, TDTR allows to estimate the interfacial behaviour in a clean model system of metal/substrate (like diamond or quartz etc.), with the restriction to plane substrates, but was also studied for different surface termination chemistries [23–25]. Qi [26] also conducted a first-principles study on clean and H-terminated CD interfaces. These calculations provided highest adhesion and interfacial strength for clean Al/CD compared to Al/CD:H and which show a very weak bonding according lowest interfacial strength resulting in a preclusion of bond formation between Al and H with fracture occurring without adhesive transfer. Existing experimental results in [8,27,28] provide qualitative support of the results in [26].

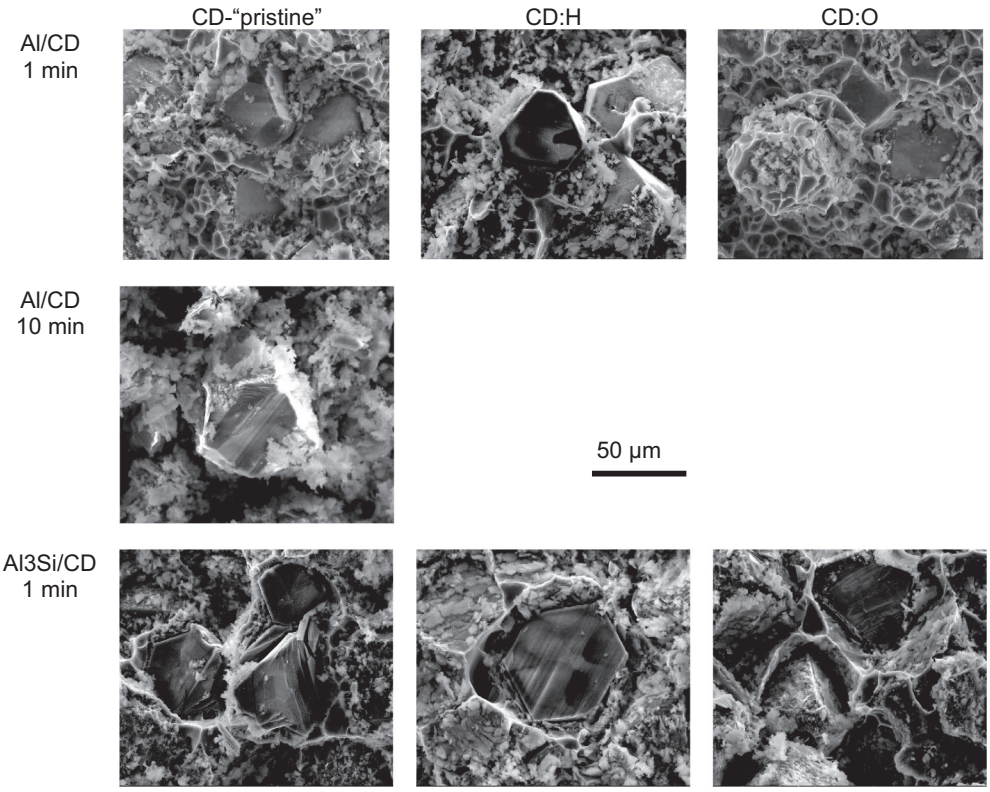

Fig. 8. Fractured surfaces of Al/CD/59p and Al3Si/CD/59p at a contact time of 1 min and 10 min respectively and different surface terminations of the diamonds before infiltration.

Although TDTR and first-principle calculations may provide a fair basis for the evaluation of the interfacial behaviour, such results are based on clean model systems and can be limited transferable to “real” composites using diamond particles of different sizes and undefined surface characteristics produced under somehow “messy” lab conditions in an autoclave or similar. However, indirect determination of interfacial bonding strength through flexural or bending strength, as well as tensile strength and compressive strength, may also provide an example for sufficient and poor interfacial adherence between the constituents in composites and has been investigated for diamond/metal composites with different coatings of diamonds and similar [15,29–31]. As shown by Chen [15], bending strength of Al/CD is a function of coating thickness, with a maximum in strength for a 45 µm W coating and a sharp decrease for smaller and larger coating thicknesses, respectively. Zhang [30] showed similar for Ti coating thicknesses on diamond. Weidenmann [31] investigated diamond composites with different matrices, including Al and different diamond particle sizes. Obviously the size had little influence on stiffness and strength, but the fracture toughness was increased by larger diamond particles. Abyzov [29] has performed a plethora of experimental investigations concerning thermal and mechanical properties of various composites. Naidich [32] also reported about the effect of different coatings, coating thickness, temperature and graphitization on the strength of contact between diamond and metal when brazing diamonds to metals.

To conclude, all the TDTR experimental results and first-principle calculations clearly demonstrate that atomic-scale details of the interfacial bonding must have a strong impact on the interfacial thermal conductances $h_{1\to2}$ through the phonon transmission coefficients $\alpha_{1\to2}$ (Eg. Eq. (4)), moreover experimentally verified on metal/diamond interfaces by [8,25], Au/quartz interfaces [23] and Al/SiC [33], respectively. Interfacial layers between matrix and inclusions in MMCs, their chemical nature, crystallinity and thickness, cleanliness and surface roughness, existence of covalent bonds etc. affects ITC and can be crucial for an efficient heat transfer between matrix and inclusions. It is also reported that oxygenated diamond surfaces can have four times higher ITC than hydrogenated ones [8,25], however, there might be some differences that can be attributed to differences in surface termination by using different acids or plasma treatments. Moreover, it must be clear again, that those investigations are related to clean model systems and might be limited comparable to composites produced by infiltration.

Anyhow, although not directly compatible with our experimental setup, the mechanical property data generated by mechanical test (flexural, bending, tensile tests) is fairly in line with our experimental findings above, as we have shown that both as-received diamonds and CD:H termination can show poor adhesion between the constituents and thus transfer of forces. This is also oppositionless to our findings, that an increase in interfacial carbide layer thickness – induced by an increasing time of contact during infiltration – results in an increase in load before (at least partial) delamination of the constituents and subsequent fracture. The same is true for the change of the matrix by the addition of Si to Al, which also results in an increase in fracture load. Note, that CD: O termination provokes similar effects.

To further elucidate and correlate our above findings with previous results in the open literature, we performed theoretical predictions for the interfacial conductance h through the phonon transmission coefficients $\alpha_{1\to2}$ by applying acoustic AMM and diffuse mismatch DMM models. This may pave the way to analyse and understand the interfacial behaviour of different interface couples in the context of mechanical properties and bonding strength of our findings.

Data for bulk and shear modulus, density and heat capacity of Al_4SiC_4 are from [34–36], diamond and Si data are from [37], for Al_4C_3 see [38]. The intrinsic thermal conductivities of Al_4SiC_4, Al_4C_3, SiC and Si are taken from [39,40], respectively, data for SiC are from [41].

The given effective sound velocities in Table 2 are calculated according Eq. (3). Note, that the given physical data for the interfacial Al-carbides are also in fair accordance with first-principle calculations

Table 2
Properties of involved materials and different interfacial products necessary for the calculation of the interfacial conductances according AMM and DMM schemes. B_i, G_i, and υ_i are the bulk and shear moduli (in Pa) and the volumetric heat capacity (in J m^{-3} K^{-1}), ρ_i the density (in kg m^{-3}), and $\upsilon_{l,i}$, $\upsilon_{t,i}$ and υ_i are the longitudinal, transversal, and effective sound velocities (m s^{-1}). The sub-index i represents each particular material.

Material	Bulk Modulus B_i	Shear modulus G_i	Densityρ_i	Volumetric heat capacity c_i	Longitudinal sound velocity $\upsilon_{l,\,i}$	Transversal sound velocity $\upsilon_{l\,t,\,i}$	Effective sound velocity υ_i	Thermal conductivity κ_i
	(Pa)	(Pa)	(kg m^{-3})	(J m^{-3} K^{-1})	(m s^{-1})	(m s^{-1})	(m s^{-1})	(W m^{-1} K^{-1})
Al_4C_3	1.70E+11	1.29E+11	2360	1.91E+06	12,038	7393	8306	107.8
Al_4SiC_4	1.79E+11	1.40E+11	3030	2.39E+06	10,986	6797	7627	80
SiC	2.13E+11	1.87E+11	3210	2.15E+06	12,001	7633	8525	77.5
Si	9.80E+10	5.20E+10	2329	1.66E+06	8476	4725	5384	148
Al	7.60E+10	2.60E+10	2700	2.44E+06	6402	3103	3595	235
Diamond	4.42E+11	4.78E+11	3515	1.78E+06	17,523	11,661	12,923	1587

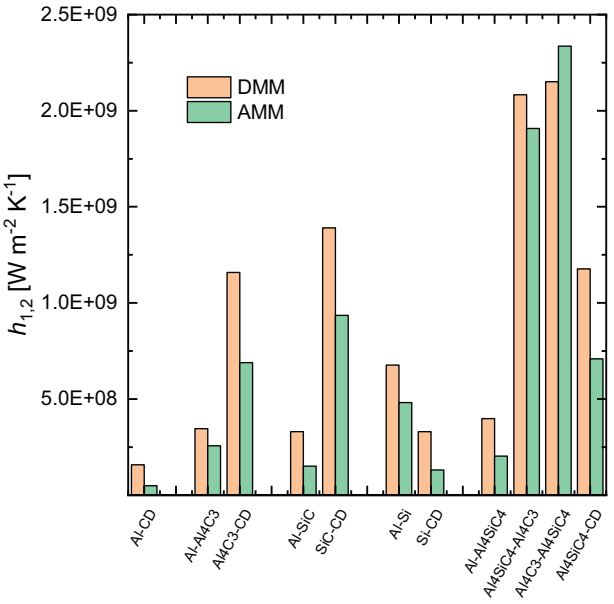

Fig. 9. Calculated interface thermal conductance $h_{1\rightarrow2}$ of different interfacial couples applying DMM and AMM schemes.

given by [42].

For both the AMM and the DMM, $h_{1\rightarrow2}$ can be estimated based on the Debye-model for the phonon density of states as

$$h_{1\rightarrow2}(\mathrm{DMM}) \approx \frac{1}{4} c_1 \rho_1 \nu_1 \alpha_{1\rightarrow2} \tag{4}$$

where $(c_1\rho_1)$ is the volumetric heat capacity (ρ is the density, c is the Debye specific heat) of material 1 (matrix) at temperature T, and $\alpha_{1\rightarrow2}$ the phonon transmission probability coefficient, andν is the linear phonon dispersion of sound speed given by

$$\nu = \left\{ \frac{1}{3} \left(\frac{1}{\nu_l^2} + \frac{2}{\nu_t^2} \right) \right\}^{-1/2} \tag{5}$$

with ν_l the longitudinal phonon velocity and ν_t is the transverse phonon velocity.

Unfortunately for most materials the numeric sound velocity values are not available, thus, they can be calculated from their elastic constants, i.e. bulk modulus B_i and shear modulus G_i according.

$$\nu_{l,1} = \left(\frac{B_1 + \frac{4}{3} G_1}{\rho_1} \right)^{1/2} \text{ and } \nu_{t,1} = \left(\frac{G_1}{\rho_1} \right)^{1/2} \tag{6}$$

$$\alpha_{1\rightarrow2} = \frac{\nu_1^2}{\nu_1^2 + \nu_2^2} \tag{7}$$

The derivation of the basic equation of phonon transport across an interface is the same for the AMM and DMM models, the only difference between the two is in the transmission coefficient $\alpha_{1\rightarrow2}$. The AMM treats the interface transfer problem in terms of continuum mechanics; an incoming elastic phonon wave at an interface can only be transmitted if it arrives at an angle within a critical cone, otherwise the wave undergoes total reflection. Furthermore, elastic waves arriving within the critical cone can be reflected or transmitted, depending on the acoustic impedance of the two continua forming the interface.

The AMM evaluates $\alpha_{1\rightarrow2}$ by solving the continuum elasticity equations for the acoustic transmission and reflection between two linear elastic solids. Because this approach ignores the granularity of the lattice, it is most appropriate for $T \leq 30$ K [43,44]:

$$h_{1\rightarrow2}(\mathrm{AMM}) = 0.5 \frac{c_1 \rho_1 \nu_1^2 \rho_2 \nu_2}{(\rho_1 \nu_1 + \rho_2 \nu_2)^2} \left(\frac{\nu_1}{\nu_2} \right)^2 \tag{8}$$

Calculations from AMM describe the ITC accurately when there is little difference in acoustic impedances between media and the Debye contrast $\Theta_{D,M}/\Theta_{D,C}$ being the metal and ceramic Debye temperatures, respectively, of approx. 0.15. Unfortunately, there can be one order of magnitude discrepancy between experimental results and predictions for materials with different acoustic properties or the Debye contrast being below or above 0.15, resulting in an under-, and overestimation of experimental h values. Considering the Debye temperatures of aluminium (428 K) and diamond (2230*K*), the AMM predictions can differ from the DMM ones by roughly a factor of 3 [38]. Modifications have been made to the above mentioned models to account for surface roughness [45], electron-phonon interactions and electron-impurity scattering [46], inelastic scattering at the interface [47] and scattering near the interface [48]. There is an increase in complexity as more features describing the interface are considered.

Fig. 9 and Table 3 display the calculated $h_{1\rightarrow2}$ according AMM and DMM schemes of different possible interface couples between interfacial carbides like Al_4C_3, SiC and Al_4SiC_4, respectively, and Al matrix and diamond. It is clear, that the ITC between Al and CD is lowest

Table 3
Calculated phonon transmission coefficient $\alpha_{1\rightarrow2}$ at the interface between material 1 and 2 and calculated interfacial conductances $h_{1\rightarrow2}$ for different realized interface couples according AMM and DMM schemes.

Interface	$\alpha_{1\rightarrow2}$	ITC $h_{1\rightarrow2}$ (DMM) (W m^{-2} K^{-1})	ITC $h_{1\rightarrow2}$ (AMM) (W m^{-2} K^{-1})
Al/CD	0.0718	1.58E8	4.93E7
Al/Al_4C_3	0.1578	3.46E8	2.57E8
Al_4C_3/Al_4SiC_4	0.5425	2.15E9	2.34E9
Al_4SiC_4/CD	0.2583	1.18E9	7.09E8
Al/Al_4SiC_4	0.1818	3.99E8	2.03E8
Al_4C_3/CD	0.2923	1.16E9	6.90E8
Al_4SiC_4/Al_4C_3	0.4575	2.08E9	1.91E9
Al/SiC	0.1510	3.31E8	1.51E8
SiC/CD	0.3032	1.39E9	9.36E8
Al/Si	0.3084	6.76E8	4.81E8
Si/CD	0.1479	3.30E8	1.31E8

compared to but all other couples like Al/Al_4C_3, Al/Al_4SiC_4, Al_4C_3/CD, Al_4C_3/Al_4SiC_4 and Al_4SiC_4/CD, which can have an ITC of an order of magnitude higher than the plane Al/CD interface. Generally, the DMM scheme also predicts higher ITCs for all interfaces than the AMM, except the Al_4C_3/Al_4SiC_4 couple. Interestingly, the couple Al_4C_3/CD and Al_4SiC_4/CD exhibit by far the highest conductances and are only outperformed by the Al_3C_4/Al_4SiC_4 interface. Unfortunately the AMM and DMM models do not allow the prediction of metal(carbide)/CD:H and metal(carbide)/CD:O interfaces and which would be of high interest for additional interpretation of the above tensile test results.

The overall ITC of the metal/CD composite with multiple interface layers, i.e. matrix/carbide(s)/CD may be calculated applying the concept of interfacial thermal resistance ITR based on a serial electrical resistivity analogy [48–51], in which the number of (carbide) layers can be easily adapted according to the number of possible reaction products at the interface:

$$\frac{1}{h_{\text{total}}} = \sum \frac{1}{h_{\text{i}\rightarrow\text{j}}} + \sum \frac{l_{\text{i}}}{\kappa_{\text{i}}} \tag{6}$$

The subscript i refers here to any of the possible interfacial compounds of a thickness l_i and a thermal conductivity κ_i, $1/h_{i\rightarrow j}$ is the interface thermal resistance of two involved materials i and j having a joint interface. In this work, such a typical series of imaginable interfacial couples can be Al/Al_4C_3/CD, Al/SiC/CD and Al/Al_4C_3/Al_4SiC_4/CD.

As shown by [49] and given by Eq. (6) the variation of the interfacial layer thickness l_i results in an increase in ITR (and conversely a decrease in ITC) und thus a deterioration in composite thermal conductivity with increasing layer thickness. This detrimental behaviour is known from composite conductivities measurements and also proven by the results given in Table 1, manifested by an increasing concentration of Al_4C_3 while increasing the contact time. The layer thickness was also determined in [6] to be dependent from the processing conditions, as it increases from 0.3–2.2 μm to 4.4–9.1 μm when changing the contact time from 1 min to 10 min.

Fig. 10 shows the results of such calculations, indicating that the interfacial layer thickness should be strictly controlled, as generally a very sharp decrease in $h_{i\rightarrow j}$ can be observed, amounting to a factor of 10

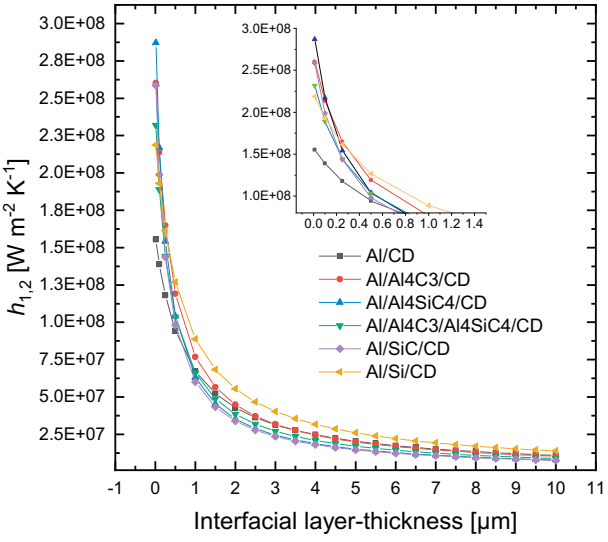

Fig. 10. Overall interface thermal conductance h between Al and diamond as a function of the interfacial layer thickness assembled from carbides like Al_4C_3, SiC and Al_4SiC_4 in the serial interface couple metal/diamond and metal/carbide (s)/diamond, respectively and calculated via the DMM model. The inset shows a (theoretically) superior behaviour of an Al/Al_4SiC_4/CD layer sequence below approx. 0.15 μm overall layer thickness, but an increased ITC for Al/Si/CD at larger interfacial thicknesses.

when increasing the interface thickness l_i from 0.1 μm to approx. 1 μm. When further increasing l the ITCs of all couples converge with each other. Furthermore, there is a ranking in h for the couples Al/CD > Al/Si/CD > Al/Al_4C_3/Al_4SiC_4/CD > Al/Al_4C_3/CD > Al/SiC/CD > Al/Al_4SiC_4/CD from lowest to highest h at infinitely small l (see inset in Fig. 10), in which both couples Al/Al_4C_3/CD and Al/SiC/CD have equivalent h. Interestingly this sequence changes at l > 0.15 μm (approx.), as then Al/Al_4C_3/CD exhibits a higher ITC than Al/Al_4SiC_4/CD and the Al/SiC/CD couple, which shows a very sharp decrease compared to the others. Furthermore, the Al/Si/CD couple is a bit out of the ordinary, as it gives the highest ITC at larger thicknesses, but this couple is quite unlikely, as Si has only a certain solubility in Al and should not exist as a pure substance at the interface (theoretically, according Eg. 2 this could be within the realms of possibility). Note that a change of the matrix from Al to Al3Si result in negligible small changes in the overall ITC of the Al(3Si)/CD couple and are thus not considered in Fig. 10. Also note, that the calculation performed for two interfacial carbides in a layer (viz. Al/Al_4C_3/Al_4SiC_4/CD) we assumed a thickness ratio between both carbides of 1:1.

When comparing the calculated h (DEM) in Table 1 with h (DMM) results in Fig. 10 we can observe a reasonable accordance between the different models. Furthermore, assuming approx. h (DEM) = 2.5E+7 W m^{-2} K^{-1} for an Al/CD:H interface (Table 1), the graph in Fig. 10 will give an interface layer thickness of approx. 4 μm and which is in fair agreement with measured carbide layer thicknesses of 0.3–2 μm for a contact of 1 min [6]. The same holds for a contact of 10 min when the corresponding carbide layer thickness of 8 μm for a ITC of 1.34E+7 in Fig. 10 conforms with the 4.4–9.1 μm in real measured Al/Al_4C_3/CD interfaces in [6].

However, compared to calculations in [48] there is an order of magnitude difference in h to our findings, but a very well accordance to the findings in [4], as well as in [25,52]. Note, that the results in [25,52] refer to a clean-model systems of sputtered Al films on plane and large CD crystals, rather than a somehow messy diamond surface condition of a gas pressure assisted infiltration setup.

4. Summary

Thermal conductivity measurements, quantitative analysis of interfacial carbides formation and neutron diffraction experiments on Al/CD and Al3Si/CD composites were reconciled to create different interfacial conditions. Both the contact time during processing the MMCs by liquid metal infiltration and the nominal composition of the matrix were changed to create different amounts of interfacial Al_4C_3 carbides, which also provokes different thicknesses of interfacial carbide layers. Moreover, different diamond surface conditions like CD:H hydrogenation and CD:O oxygenation were realized to compare with the untreated, “pristine”, surface condition of diamond particles.

Neutron diffraction showed both, the increase in contact time and the addition of Si to Al increase the bonding strength. The increase in contact time is also associated with an increase in interfacial carbide layer thickness (and equivalent an increase in Al_4C_3 carbide concentration) and which is closely connected to a higher load transfer from the ductile metallic matrix into the diamond particles, as this obviously improves bonding strength between matrix and diamonds. The same effect is observed for Al3Si matrix and or a contact time of 1 min and which also results in increased bonding strength comparable to a contact time of 10 min in the pure Al/CD system. Moreover, an Al3Si matrix also causes a decrease in interfacial carbides concentration; unfortunately this is also associated to a significant decrease in composite thermal conductivity.

In general, we observed elasto-plastic deformation of the matrix up to maximum strains, followed by decrease in matrix strain, which can be explained by plastic deformation leading to matrix damage and partial delamination at the diamond-metal interfaces. Concomitantly the diamonds are linearly fully elastic deformed until rupture without

any peak and decrease in strain. No total delamination between the constituents is evident, as diamonds would not linearly deform until rupture, if there is full delamination. The elastic deformation of diamonds relies on certain residual adhesion forces between diamond and matrix, since otherwise no forces could be transmitted with further increasing load.

When we introduce different surface terminations on diamond surfaces the deformation behaviour is different, as the fracture load increases for CD:O compared to pristine and CD:H terminated ones. This is consistent with thermo-physical property results, where the Al:O composite has a significantly higher thermal conductivity compared to the pristine and CD:H terminated ones.

The plastically deformed Al matrix shows a network of dimples in the fracture surfaces, typical for the ductile behaviour of pure metals. All interfaces between matrix and diamond particles show sufficient interfacial bonding, except the Al/CD-pristine 1 min composite, which exhibits partly unaffected diamond planes. Al3Si/CD exhibit no dimples, but a Si skeleton in the Al phase is visible.

Furthermore, we performed theoretical predictions for the interfacial conductance h by applying AMM and DMM models to compare with experimental thermophysical results and DEM calculations. These results demonstrate the dependence of h on interlayer structure, which may also pave a future way for interfacial design in Al/CD composites. Theoretically the presence of a SiC/CD interface should be favourable, as this conductance is significantly higher than the Al_4C_3/CD and, moreover, the Al/CD pair. Considering spatial resolution of interfaces and different sequences of possible interfacial carbidic reaction products between Al, Si and CD, theoretically, the presence of Al_4SiC_4 close to the CD interface appears to be favourable.

Funding

This research did not receive any specific grant from funding agencies in the public, commercial, or not-for-profit sectors.

CRediT authorship contribution statement

Edtmaier Christian:Writing - original draft, Conceptualization, Data curation, Validation, Formal analysis, Supervision.**Segl Jakob**:Investigation, Resources, Data curation, Formal analysis.**Robert Koos**:Investigation, Resources, Data curation.**Michael Schöbel**:Writing - review & editing.**Christoph Feldbaumer**:Investigation, Resources, Data curation.

Declaration of competing interest

The authors declare that they have no known competing financial interests or personal relationships that could have appeared to influence the work reported in this paper.

References

[1] M. Schöbel, W. Altendorfer, H.P. Degischer, S. Vaucher, T. Buslaps, M.D. Michiel, M. Hofmann, Internal stresses and voids in SiC particle reinforced aluminum composites for heat sink applications, Compos. Sci. Technol. 71 (2011) 724–733.
[2] M. Schöbel, H.P. Degischer, S. Vaucher, M. Hofmann, P. Cloetens, Reinforcement architectures and thermal fatigue in diamond particle-reinforced aluminum, Acta Mater. 58 (2010) 6421–6430.
[3] M. Kouzeli, L. Weber, C. San Marchi, A. Mortensen, Quantification of microdamage phenomena during tensile straining of high volume fraction particle reinforced aluminium, Acta Mater. 49 (2001) 497–505.
[4] I.E. Monje, E. Louis, J.M. Molina, Optimizing thermal conductivity in gas-pressure infiltrated aluminum/diamond composites by precise processing control, Compos. A: Appl. Sci. Manuf. 48 (2013) 9–14.
[5] I.E. Monje, E. Louis, J.M. Molina, Aluminum/diamond composites: a preparative method to characterize reactivity and selectivity at the interface, Scr. Mater. 66 (2012) 789–792.
[6] C. Edtmaier, J. Segl, E. Rosenberg, G. Liedl, R. Pospichal, A. Steiger-Thirsfeld, Microstructural characterization and quantitative analysis of the interfacial carbides in Al(Si)/diamond composites, J. Mater. Sci. 53 (2018) 15514–15529.
[7] P.W. Ruch, O. Beffort, S. Kleiner, L. Weber, P.J. Uggowitzer, Selective interfacial bonding in Al(Si)–diamond composites and its effect on thermal conductivity, Compos. Sci. Technol. 66 (2006) 2677–2685.
[8] C. Monachon, L. Weber, Influence of diamond surface termination on thermal boundary conductance between Al and diamond, J. Appl. Phys. 113 (2013) 183504.
[9] C. Edtmaier, E. Bauer, L. Weber, Z.S. Tako, J. Segl, G. Friedbacher, Temperature dependence of the thermal boundary conductance in Ag–3Si/diamond composites, Diam. Relat. Mater. 57 (2015) 37–42.
[10] C. Edtmaier, E. Bauer, J. Segl, A. Foelske-Schmitz, L. Pambaguian, 46th International Conference on Environmental Systems, Texas Tech University Library, Vienna, 2016, pp. 1–14.
[11] T. Hutsch, T. Schubert, T. Weißgärber, B. Kieback, World PM 2016 Congress and Exhibition, (2016).
[12] T. Schubert, B. Trindade, T. Weißgärber, B. Kieback, Interfacial design of Cu-based composites prepared by powder metallurgy for heat sink applications, Mater. Sci. Eng. A 475 (2008) 39–44.
[13] T. Hutsch, T. Schubert, T. Weißgärber, B. Kieback, Key Eng. Mater. (2017) 151–157.
[14] O. Beffort, F.A. Khalid, L. Weber, P. Ruch, U.E. Klotz, S. Meier, S. Kleiner, Interface formation in infiltrated Al(Si)/diamond composites, Diam. Relat. Mater. 15 (2006) 1250–1260.
[15] G. Chen, W. Yang, L. Xin, P. Wang, S. Liu, J. Qiao, F. Hu, Q. Zhang, G. Wu, Mechanical properties of Al matrix composite reinforced with diamond particles with W coatings prepared by the magnetron sputtering method, J. Alloys Compd. 735 (2018) 777–786.
[16] M. Hofmann, R. Schneider, G.A. Seidl, J. Rebelo-Kornmeier, R.C. Wimpory, U. Garbe, H.G. Brokmeier, The new materials science diffractometer STRESS-SPEC at FRM-II, Phys. B Condens. Matter 385–386 (2006) 1035–1037.
[17] M. Hoelzel, W.M. Gan, M. Hofmann, C. Randau, G. Seidl, P. Jüttner, W.W. Schmahl, Rotatable multifunctional load frames for neutron diffractometers at FRM II—design, specifications and applications, Nuclear Instruments and Methods in Physics Research Section A: Accelerators, Spectrometers, Detectors and Associated Equipment 711 (2013) 101–105.
[18] J. Rebelo-Kornmeier, M. Hofmann, W.M. Gan, C. Randau, K. Braun, K. Zeitelhack, I. Defendi, J. Krueger, E. Faulhaber, H.G. Brokmeier, New developments of the materials science diffractometer STRESS-SPEC, Mater. Sci. Forum 905 (2017) 151–156.
[19] C. Randau, U. Garbe, H.-G. Brokmeier, StressTextureCalculator: a software tool to extract texture, strain and microstructure information from area-detector measurements, J. Appl. Crystallogr. 44 (2011) 641–646.
[20] J. Rebelo Kornmeier, J. Gibmeier, M. Hofmann, Minimization of spurious strains by using a Si bent-perfect-crystal monochromator: neutron surface strain scanning of a shot-peened sample, Meas. Sci. Technol. 22 (2011) 065705.
[21] Y. Yamamoto, T. Imai, K. Tanabe, T. Tsuno, Y. Kumazawa, N. Fujimori, The measurement of thermal properties of diamond, Diam. Relat. Mater. 6 (1997) 1057–1061.
[22] M. Schöbel, P. Dobron, J. Bernardi, R. Wimpory, K. Weidenmann, Elasto-plastic deformation within diamond reinforced metals for thermal management, Diam. Relat. Mater. 70 (2016) 52–58.
[23] M.D. Losego, M.E. Grady, N.R. Sottos, D.G. Cahill, P.V. Braun, Effects of chemical bonding on heat transport across interfaces, Nat. Mater. 11 (2012) 502–506.
[24] C. Monachon, L. Weber, C. Dames, Thermal boundary conductance: a materials science perspective, Annu. Rev. Mater. Res. 46 (2016) 433–463.
[25] K.C. Collins, S. Chen, G. Chen, Effects of surface chemistry on thermal conductance at aluminum-diamond interfaces, Appl. Phys. Lett. 97 (2010) 083102.
[26] Y. Qi, L.G. Hector, Adhesion and adhesive transfer at aluminum/diamond interfaces: a first-principles study, Phys. Rev. B 69 (2004) 235401.
[27] C. Monachon, G. Schusteritsch, E. Kaxiras, L. Weber, Qualitative link between work of adhesion and thermal conductance of metal/diamond interfaces, J. Appl. Phys. 115 (2014) 123509.
[28] P.M. Norris, J.L. Smoyer, J.C. Duda, P.E. Hopkins, Prediction and measurement of thermal transport across interfaces between isotropic solids and graphitic materials, J. Heat Transf. 134 (2011) 20910.
[29] A.M. Abyzov, F.M. Shakhov, A.I. Averkin, V.I. Nikolaev, Mechanical properties of a diamond–copper composite with high thermal conductivity, Mater. Des. 87 (2015) 527–539.
[30] H. Zhang, J. Wu, Y. Zhang, J. Li, X. Wang, Y. Sun, Mechanical properties of diamond/Al composites with Ti-coated diamond particles produced by gas-assisted pressure infiltration, Mater. Sci. Eng. A 626 (2015) 362–368.
[31] K.A. Weidenmann, R. Tavangar, L. Weber, Mechanical behaviour of diamond reinforced metals, Mater. Sci. Eng. A 523 (2009) 226–234.
[32] Y.V. Naidich, V.P. Umanskii, I.A. Lavrineko, Strength of the Diamond-Metal Interface and Brazing of Diamonds, Cambridge International Science Publishing Ltd, Cambridge, 2007.
[33] C.-W. Nan, X.-P. Li, R. Birringer, Inverse problem for composites with imperfect Interface: determination of interfacial thermal resistance, thermal conductivity of constituents, and microstructural parameters, J. Am. Ceram. Soc. 83 (2000) 848–854.
[34] R.P. Beyer, E.A. Johnson, Heat capacity of aluminum silicon carbide (Al4SiC4) from 5.26 to 1047 K, J. Chem. Thermodyn. 16 (1984) 1025–1029.
[35] L. Pedesseau, J. Even, M. Modreanu, D. Chaussende, E. Sarigiannidou, O. Chaix-Pluchery, O. Durand, Al4SiC4 wurtzite crystal: Structural, optoelectronic, elastic, and piezoelectric properties, APL Materials 3 (2015) 121101.
[36] T. Liao, J. Wang, Y. Zhou, Atomistic deformation modes and intrinsic brittleness of Al4SiC4: a first-principles investigation, Phys. Rev. B 74 (2006) 174112.

[37] N.N., C-diamond, Mechanical Properties, Elastic Constants, Lattice Vibrations, http://www.ioffe.ru/SVA/NSM/Semicond/Diamond/mechanic.html.
[38] I.E. Monje, E. Louis, J.M. Molina, Role of Al4C3 on the stability of the thermal conductivity of Al/diamond composites subjected to constant or oscillating temperature in a humid environment, J. Mater. Sci. 51 (2016) 8027–8036.
[39] K. Inoue, S. Mori, A. Yamaguchi, Thermal conductivity and temperature dependence of linear thermal expansion coefficient of Al4SiC4 sintered bodies prepared by pulse electronic current sintering, J. Ceram. Soc. Jpn. 111 (2003) 348–351.
[40] B. Ma, J. Wang, T.H. Lee, S.E. Dorris, J. Wen, U. Balachandran, Microstructural characterization of Al4C3 in aluminum–graphite composite prepared by electron-beam melting, J. Mater. Sci. 53 (2018) 10173–10180.
[41] R. Gaillac, P. Pullumbi, F.-X. Coudert, ELATE: an open-source online application for analysis and visualization of elastic tensors, J. Phys. Condens. Matter 28 (2016) 275201.
[42] L. Sun, Y. Gao, Y. Li, K. Yoshida, T. Yano, D. Yi, Structural, bonding, anisotropic mechanical and thermal properties of Al4SiC4 and Al4Si2C5 by first-principles investigations, Journal of Asian Ceramic Societies 4 (2016) 289–298.
[43] E.T. Swartz, R.O. Pohl, Thermal resistance at interfaces, Appl. Phys. Lett. 51 (1987) 2200–2202.
[44] E.T. Swartz, R.O. Pohl, Thermal boundary resistance, Rev. Mod. Phys. 61 (1989) 605–668.
[45] G. Dharmadurai, Influence of surface characteristics of solids on the Kapitza resistance, Physica B+C 115 (1983) 229–232.
[46] P.M. Echternach, M.E. Gershenson, H.M. Bozler, Evidence of interference between electron-phonon and electron-impurity scattering on the conductivity of thin metal films, Phys. Rev. B 47 (1993) 13659–13663.
[47] A.V. Sergeev, Electronic Kapitza conductance due to inelastic electron-boundary scattering, Phys. Rev. B 58 (1998) R10199–R10202.
[48] M. Battabyal, O. Beffort, S. Kleiner, S. Vaucher, L. Rohr, Heat transport across the metal–diamond interface, Diam. Relat. Mater. 17 (2008) 1438–1442.
[49] Z. Tan, Z. Li, D.-B. Xiong, G. Fan, G. Ji, D. Zhang, A predictive model for interfacial thermal conductance in surface metallized diamond aluminum matrix composites, Mater. Des. 55 (2014) 257–262.
[50] Y. Zhang, H.L. Zhang, J.H. Wu, X.T. Wang, Enhanced thermal conductivity in copper matrix composites reinforced with titanium-coated diamond particles, Scr. Mater. 65 (2011) 1097–1100.
[51] W. Yang, G. Chen, P. Wang, J. Qiao, F. Hu, S. Liu, Q. Zhang, M. Hussain, R. Dong, G. Wu, Enhanced thermal conductivity in diamond/aluminum composites with tungsten coatings on diamond particles prepared by magnetron sputtering method, J. Alloys Compd. 726 (2017) 623–631.
[52] C. Monachon, L. Weber, Effect of diamond surface orientation on the thermal boundary conductance between diamond and aluminum, Diam. Relat. Mater. 39 (2013) 8–13.